IDENTIFICATION OF THE BIOMECHANICAL BEHAVIOR OF A ROTORCRAFT PILOT ARM

M. Mattaboni[⋆], A. Fumagalli[⋆], G. Quaranta[⋆] and P. Masarati[⋆]

[⋆]Dipartimento di Ingegneria Aerospaziale
Politecnico di Milano, Campus Bovisa, Via La Masa 34, 20156 Milano, Italy
e-mail: mattaboni@aero.polimi.it,
web page: http://www.aero.polimi.it/

Keywords: Rotorcraft Aeromechanics, Pilot Biomechanics, Aeroservoelasticity, Multibody Dynamics

Abstract. *This paper addresses the identification of the equivalent mechanical properties of a helicopter pilot. A multibody model of the kinematics of the upper limb is used to describe the motion of the left arm holding the collective control stick. Geometric and inertia properties are obtained computing regression equations on anthropometric surveys, considering the pilot's weight and height. The multibody model of the pilot's upper limb is required to analyze the involuntary participation of the pilot to the injection into the control system of the motion induced by the aircraft's vibrations. The proposed method is validated using generated data. Its robustness is illustrated and discussed. No conclusive results have been obtained using measured data. Possible causes are discussed as well.*

1 INTRODUCTION

Pilot biomechanics modeling received significant attention in the literature. One of the reasons is the essential role it plays in the so-called Pilot-Augmented Oscillations (PAO), a form of Aircraft-Pilot Coupling (APC) that involves the unintended participation of the pilot in sustaining and amplifying oscillations of aeroelastic nature in a range of frequencies higher that those a human being is supposed to be able to intentionally counteract [1]. This type of phenomena is well-known in fixed wing aircraft, but its occurrence has been reported in rotary wing ones as well [2].

Pilot biomechanics modeling represented the subject of extensive research, especially with reference to fixed wing aircraft, as soon as performance improvements and significantly the introduction of Automatic Flight Control Systems (AFCS) and Fly-By-Wire (FBW) raised the pass band frequency of flight controls [3, 4].

Similar trends may be observed in the rotorcraft field, although a little later. Rotorcraft present peculiarities with respect to fixed wing aircraft. Some of them are related to a different layout of the controls, significantly of the collective control stick and the dynamics it controls [5]. The simulation of unconventional rotorcraft configurations, like tiltrotors, with a mix of conventional collective control stick and Thrust Control Lever (TCL), may require special care as well in modeling the passive interaction with the pilot [6, 7].

Recently, the problem was investigated in Europe by the GARTEUR HC AG-16 project. Among the results of this activity, the importance of considering the pilot biomechanics when modeling rotorcraft aeroservoelasticity emerged as a strong indication [8, 9].

This work presents some results of an activity aimed at identifying the properties of biomechanical models of rotorcrafy pilots. The multibody modeling of the pilot's biomechanical behavior is presented first, addressing issues like the initial placement of the model in the cockpit with the desired configuration, and the reconstruction of the kinematics from measures, including the case of redundant measures. The problem of determining suitable constitutive models of the articulations is discussed. An approach based on power balance fitting is proposed. Its application to a set of numerical problems is illustrated, and its applicability to experimental results is discussed.

2 MULTIBODY MODELING OF THE PILOT

To model the pilot's biomechanics in detail, a multibody model of the pilot has been developed. The aim is to provide a detailed biodynamic model that allows the simulation of the pilot's behavior based on first principles, exploiting the knowledge of accurate kinematic and inertial properties of limbs and articulations, completed by impedance properties of relevant articulations obtained from dedicated measurements. This is expected to allow realistic simulations of the behavior of the pilot without the need to refer to a specific reference condition, as required when using standard linear transfer functions.

A complete kinematic model of the pilot's body has been developed [10]. A kinematic procedure has been defined for the initial placement of the pilot inside the helicopter cockpit. This procedure is required to correctly compute the initial posture of the pilot within the cockpit. In fact, the collective and cyclic sticks need to be grabbed by the pilot while sitting on the seat, with the feet correctly placed on the pedals and the torso lying on the back of the seat.

In this preliminary phase, since the main objective of this work is to study the pilot-collective interaction, the model of the arm grabbing the collective is extracted and isolated. This is required, because the only available experimental data consists in measurements related to the

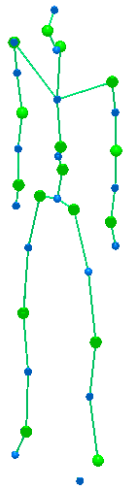

Figure 1: Sketch of the multibody model of the pilot in the initial configuration. The larger spheres represent the articulations, while the smaller ones are located at the center of mass of the limbs.

orientation and acceleration of the left upper limb, the absolute motion of the seat and the relative motion of the collective stick.

An attempt is made to use the model to identify meaningful biomechanical parameters starting from the experimental data described in [11].

2.1 The Pilot Model

The multibody model of the pilot is made of a set of rigid bodies representing limbs, hands, feet, torso and the head, and by a set of joints representing the articulations. The model consists in:

- geometric properties: the points where limbs connect, the relative orientation of the limbs, and the relative motions allowed by each articulation;
- inertial properties: estimated mass, center of gravity location and moments of inertia of each limb;
- impedance properties of the muscles at each articulation; this information is seldom available in a manner that allows to build a multibody model of a human body the way this model is usually intended, since the impedance of the muscles may depend on a number of factors that are beyond the simulation capability of conventional mechanical simulation software: muscular activation level, pilot's workload, pilot's fatigue, pilot's attention, and more. The identification of those properties is the objective of this analysis.

Most of this data depends on the size of the pilot; a gross distinction is based on the sex, the age (child or adult), the height and the weight of the individual. There exist databases that provide this type of information based on statistics (see e.g. [12]).

A sketch of the model is shown in Figure 1. Rigid bodies and articulations are represented as blue and green spheres; respectively. The model is made of 17 rigid bodies, detailed in Table 1, and by 16 joints, detailed in Table 2.

Numerical data used in the model for the geometry of the body (limbs length, mass and inertia moments) have been obtained using a tool named FEBOD based on a statistical biometric database called GEBOD, illustrated in [12]. This tool provides estimated biometric parameters

Table 1: Multibody model of the pilot: rigid bodies modeling limbs.

Rigid Bodies	Description
1	Head
1	Neck
3	Lower, central and upper torso
4	Right/Left lower and upper arms
2	Right/Left hands
4	Right/Left lower and upper legs
2	Right/Left feet
17	Total

Table 2: Multibody model of the pilot: joints modeling articulations.

Joints	Name	Connecting	Joint Type
1	Upper Neck	Head - Neck	Spherical Hinge
1	Lower Neck	Neck - Upper Torso	Spherical Hinge
2	Right/Left Shoulder	Upper Torso - Upper Arms	Spherical Hinge
2	Right/Left Elbow	Upper - Lower Arms	Revolute Hinge
2	Right/Left Wrist	Lower Arms - Hands	Spherical Hinge
1	Waist	Upper - Central Torso	Spherical Hinge
1	Pelvis	Central - Lower Torso	Spherical Hinge
2	Right/Left Hip	Lower Torso - Upper Legs	Spherical Hinge
2	Right/Left Knee	Upper - Lower Legs	Revolute Hinge
2	Right/Left Ankle	Lower Legs - Foots	Spherical Hinge
16	Total		

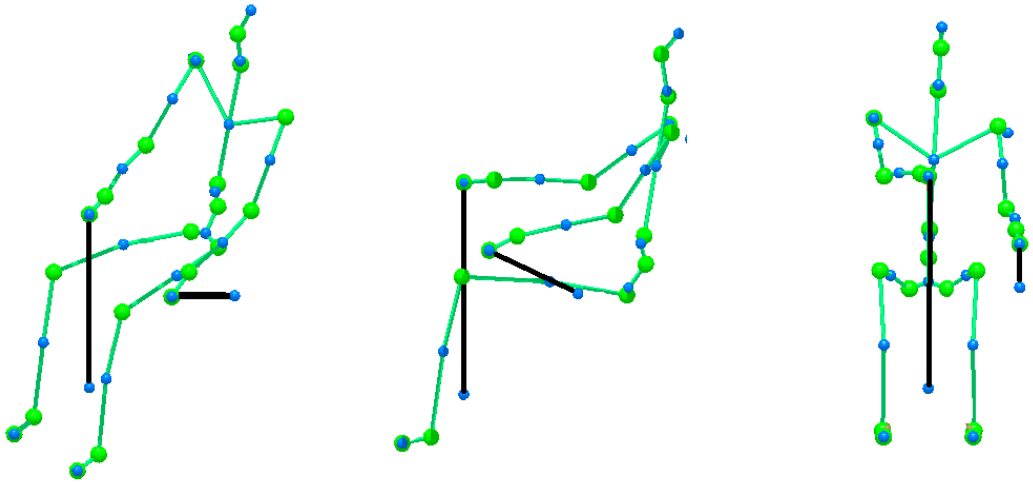

Figure 2: Sketch of the pilot model inside the cabin as resulting from the initial placement procedure.

based on the sex and age of the individual and either on the percentile or the combination of weight and height.

A parametric prototype of a multibody human has been developed, so that multiple individuals can be independently included in a single analysis by simply changing the biometric parameters and by defining the posture, namely the location and orientation of a reference point and the relative position of each articulation, if known.

2.2 Initial Placement

After the model is generated, the initial condition of the system must be computed. Since the pilot is seated inside the cabin while handling control bars, an initial configuration representing this situation needs to be computed.

The direct estimation of the relative orientation of the articulations of a pilot in a cockpit, when the size of the pilot and the desired initial position of the controls can vary, may not be a trivial task. The multibody analysis can help in this case by computing a consistent initial position.

This task is achieved by means of a kineto-static simulation during which the model, starting from an arbitrary initial configuration (the default one is depicted in Figure 1), is driven to a position consistent with the case of a pilot inside the helicopter cockpit. Multiple requirements need to be met: the pilot is seated on a helicopter seat, with seat belts fastened, holding control sticks and keeping feet on pedals at a specified initial control position.

By driving the required points of the model to the desired position, this task can be easily achieved when the cabin dimensions are known. An example of the initial configuration on the pilot inside the cockpit is depicted in Figure 2.

The kinematic procedure used to drive the model in the desired position will be described in subsequent sections, since it is analogous to the methodology used to reconstruct the motion of the pilot starting from experimental measurements.

2.3 The Arm Model

Experimental data refers to the acceleration and orientation of the arm handling the collective stick. The system is excited by the heave motion of the seat. Actually, the whole cockpit moves.

Table 3: Joint constitutive laws dimensionality.

Joint	Dimension	Free directions
Wrist	2	$X - Y$
Elbow	1	Z
Shoulder	3	$X - Y - Z$

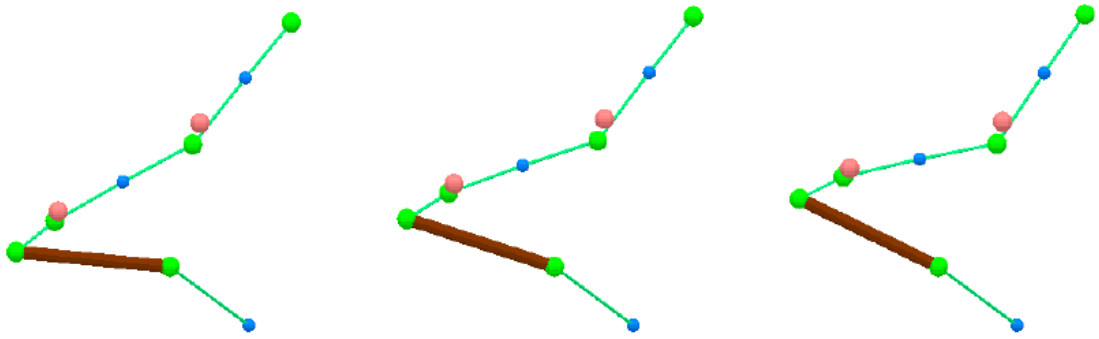

Figure 3: Sketch of the left arm grabbing the collective stick. The location of the sensors is illustrated as well.

It is assumed that the motion of the seat does not significantly differ from that of the cockpit. The objective is the motion of the arm and the rotation induced by the pilot in the collective stick. For this purpose, a simplified model of the arm is extracted from the complete pilot model, together with the collective stick, considered rigid.

The left shoulder is assumed to be rigidly attached to the seat, since in the available data no measurements of the motion of shoulder and torso were available. The collective bar can freely rotate about its hinge. This is relatively consistent with the experimental setting of friction off.

When the hand grasps the collective bar the wrist rotation around the axis connecting the wrist and the collective handle is prevented. This additional constraint is necessary to be able to reconstruct the whole motion of the system starting from the available measures. The dimensions of the constitutive laws of the joints is summarized in Table 3. A sketch of the partial model is shown in Figure 3.

2.4 Motion Reconstruction

The previously described model is used for parameter identification of the biodynamic features of the real pilot. The first step consists in reconstructing the motion of the articulations, based on available experimental measurements.

These are:

- the vertical acceleration of the seat;
- the rotation of the collective bar;
- the linear accelerations of the two MTx sensors;
- the orientation parameters of the two MTx sensors.

The MTx sensors are solid-state strapdown Inertial Measurement Units, manufactured by XSens (http://xsens.com/). They measure three components of acceleration and angular velocity

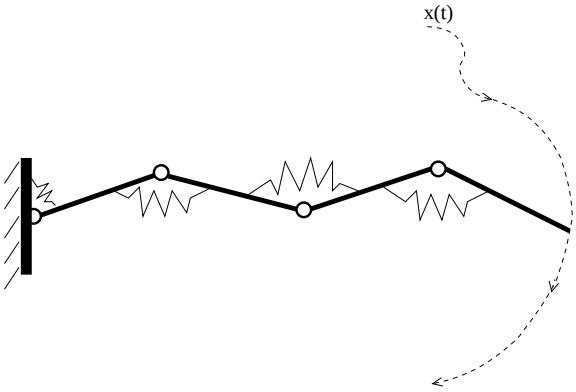

Figure 4: A planar mechanism with dummy springs.

in a reference frame attached to the sensor, and use integration in time, compensated by a measure of the Earth magnetic field, to reconstruct their absolute orientation.

A human arm has 7 Degrees of Freedom (DoFs): the rotation of the shoulder adds 3 DoFs, 1 is added by the rotation of the elbow and 3 by the rotation of the wrist.

The hand must grasp the collective stick, thus eliminating the 3 DoFs corresponding to the position of the hand, which must be coincident with a given location on the collective stick. The computation of the motion of the involved articulations is usually an under-determined kinematic problem, because only 6 movements corresponding to position and orientation of the hand are imposed to determine the 7 DoFs of the arm.

In the present case, however, the addition of the movements measured by the sensors makes the problem overconstrained, since these impose 12 additional constraints.

The kinematic solution is found using a clear physical interpretation of a least-square/pseudo-inverse methodology in terms of a kineto-static problem. The following section describes the approach, starting from kinematic inversion of redundant mechanisms (as the human arm) and proceeding with the extension to over-constrained problems.

2.4.1 Kinematic Inversion of Redundant Mechanisms

Redundancy is defined as the number of DoFs exceeding those strictly required to perform a desired task in the workspace of the mechanism. For a spatial system, 6 DoFs are required (in the present case, to impose the motion of the hand), while the human arm has 7 DoFs.

The inverse kinematics problem for redundant mechanisms is known to be ill-posed, since the problem is underdetermined. The inverse solution is usually found in an error minimization sense: among the infinite admissible solutions, the one with minimum norm is chosen. It is usually obtained via pseudo-inversion of the governing matrix.

An interesting physical interpretation can be given of the minimum norm solution of the kinematic problem when an auxiliary kineto-static system is considered.

Consider a static system composed by a kinematic mechanism with m degrees of freedom, whose joints motion $\boldsymbol{\theta}$ is reacted by a set of 'dummy' springs, as depicted in Figure 4. An arbitrary point of the system is forced to move along a specified path $\mathbf{x}(t)$, with a specified orientation, as required. This constraint is expressed as a set of non-linear relations between joint coordinates and the specified path:

$$\boldsymbol{\gamma}(\boldsymbol{\theta}) = \mathbf{x}(t). \tag{1}$$

The static equilibrium configuration of this system is computed as the the minimum of the elastic potential energy associated with the spring system under the rheonomic end-effector position constraint:

$$\min \left(\Delta\boldsymbol{\theta}^T \mathbf{K} \Delta\boldsymbol{\theta}\right) \quad \text{constrained by} \quad \boldsymbol{\gamma}\left(\boldsymbol{\theta}\right) = \mathbf{x}\left(t\right) \tag{2}$$

where $\mathbf{K}$ is the stiffness matrix of the springs. Using Lagrange multipliers and linearizing the nonlinear constraint equation, the minimization problem of Eq. (2) can be rewritten as

$$\begin{bmatrix} \mathbf{K} & \boldsymbol{\gamma}_{/\boldsymbol{\theta}}^T \\ \boldsymbol{\gamma}_{/\boldsymbol{\theta}} & \mathbf{0} \end{bmatrix} \begin{Bmatrix} \Delta\boldsymbol{\theta} \\ \boldsymbol{\lambda} \end{Bmatrix} = \begin{Bmatrix} \mathbf{0} \\ \mathbf{x}(t) - \boldsymbol{\gamma}(\boldsymbol{\theta}) \end{Bmatrix} \tag{3}$$

where $\boldsymbol{\lambda}$ is the vector of Lagrangian multipliers associated with the constraint equations. In general, it represents the constraint reactions and, in this case, it specifically represents the forces that must be applied to the end-effector to produce the motion $\mathbf{x}(\boldsymbol{t})$ in the auxiliary problem. This implies that the multipliers $\boldsymbol{\lambda}$ do not have a specific physical meaning for the actual problem, they are only meaningful with respect to the 'dummy' problem of solving the underdetermined kinematic problem.

The problem is solved by computing, at each time $\overline{t}$ of interest, the static equilibrium of the auxiliary system with the external dummy forces and moments $\boldsymbol{\lambda}$ introduced by the constraint that drives the motion of the end-effector. This system of equations can be solved for all times $\overline{t}$ of interest to find the solution of the inverse kinematics problem.

The method results in the classic Moore-Penrose pseudo-inverse of the Jacobian of the constraint matrix when an isotropic diagonal stiffness matrix is used, namely $\mathbf{K} = \alpha\mathbf{I}$. In fact, the first block row of Eq. (3) can be solved for $\Delta\boldsymbol{\theta}$, yielding

$$\Delta\boldsymbol{\theta} = -\mathbf{K}^{-1}\boldsymbol{\gamma}_{/\boldsymbol{\theta}}^T\boldsymbol{\lambda} \tag{4}$$

which, substituted in the second row, gives

$$-\boldsymbol{\gamma}_{/\boldsymbol{\theta}}\mathbf{K}^{-1}\boldsymbol{\gamma}_{/\boldsymbol{\theta}}^T\boldsymbol{\lambda} = \mathbf{x}(\overline{t}) - \boldsymbol{\gamma}(\boldsymbol{\theta}). \tag{5}$$

Matrix $\boldsymbol{\gamma}_{/\boldsymbol{\theta}}\mathbf{K}^{-1}\boldsymbol{\gamma}_{/\boldsymbol{\theta}^T}$ is square. If $\boldsymbol{\gamma}_{/\boldsymbol{\theta}}$ is not rank deficient (i.e. if the constraints are not redundant), it can be inverted to yield

$$\boldsymbol{\lambda} = -\left(\boldsymbol{\gamma}_{/\boldsymbol{\theta}}\mathbf{K}^{-1}\boldsymbol{\gamma}_{/\boldsymbol{\theta}^T}\right)^{-1}\left(\mathbf{x}(\overline{t}) - \boldsymbol{\gamma}(\boldsymbol{\theta})\right). \tag{6}$$

By back-substituting $\boldsymbol{\lambda}$ in Eq. (4), $\boldsymbol{\theta}$ results in

$$\Delta\boldsymbol{\theta} = \mathbf{K}^{-1}\boldsymbol{\gamma}_{/\boldsymbol{\theta}}^T\left(\boldsymbol{\gamma}_{/\boldsymbol{\theta}}\mathbf{K}^{-1}\boldsymbol{\gamma}_{/\boldsymbol{\theta}^T}\right)^{-1}\left(\mathbf{x}(\overline{t}) - \boldsymbol{\gamma}(\boldsymbol{\theta})\right), \tag{7}$$

which corresponds to a classical pseudo-inverse when $\mathbf{K}$ is diagonal isotropic.

If $\mathbf{K} \neq \alpha\mathbf{I}$, the spring stiffnesses can be considered free parameters that can be used as penalties on the motion of each joint in favor of other joints and, as such, they become design parameters to shape the solution. In this case, the solution of the inverse kinematics problem is computed in a weighted least squares sense: weights are directly given by assigning the stiffnesses of the dummy springs.

These parameters can be selected in order to penalize the motion of some joints in favor of others, to drive the solution towards a more natural motion of the arm. Static external forces can be added to further shape the solution. For example, the weight can be added to privilege solutions that account for gravity.

The method can be easily implemented in general purpose multibody software [13] and thus well suits the analysis of complicated systems like the human body.

2.4.2 Overconstrained System

When the number of imposed movements exceeds the number of DoFs the system is kinematically overconstrained. This means that there are more equations than unknowns.

Consider a generic linear constraint

$$\mathbf{A}\mathbf{x} = \mathbf{b}; \tag{8}$$

constraints are redundant if the row-rank r_r of matrix $\mathbf{A} \in \mathbb{R}^{c \times n}$ is less than its number of rows, c. Constraints are inconsistent when they are redundant, the column rank r_c of matrix $\mathbf{A}$ is less than the number of constraints, c, and vector $\mathbf{b} \in \mathbb{R}^c$ does not belong to the column space of matrix $\mathbf{A}$, so that Eq. (8) has no solution.

In the case under investigation, the arm is forced to move by imposing the measured motion of the collective bar, of the seat and of the sensors. In total, 19 equations are imposed:

- +1: Collective motion
- +1: Seat vertical motion
- +5: hand grasping the collective bar
- +6: 3 linear acceleration and 3 orientation parameters of the first sensor
- +6: 3 linear acceleration and 3 orientation parameters of the second sensor

In this case, a least square solution is required. Also this task can be obtained by the solution of an equivalent kineto-static problem. The driving constraints are imposed in a relaxed manner: instead of directly imposing a set of algebraic constraints, Eq. (1), the driving constraints are imposed as dummy elastic forces acting on the auxiliary system described earlier. The resulting equilibrium equations are:

$$\mathbf{K}\Delta\boldsymbol{\theta} = -\boldsymbol{\gamma}'^{T}_{\boldsymbol{\theta}}\mathbf{K}_c\left(\boldsymbol{\gamma}\left(\Delta\boldsymbol{\theta}\right) - \mathbf{x}\left(t\right)\right) \tag{9}$$

where matrix $\mathbf{K}$ is again the stiffness matrix of the dummy springs that react the motion of the joint. Matrix $\mathbf{K}_c$ represents a stiffness associated to a new set of dummy springs that relax the imposition of the motion. This new set of dummy springs connects the points whose motion is measured is known, i.e. the locations of the sensors, to the limbs. Note that vector $\boldsymbol{\gamma}$ has dimension $m > n$.

This allows to find the solution of the inverse kinematics problem in a least square sense: mechanism redundancy (underdetermination) is solved by matrix $\mathbf{K}$ that is used to tune the motion of the joints, the set of driving equations is solved in a way that minimizes the norm of vector $\mathbf{K}_c\left(\boldsymbol{\gamma}\left(\Delta\boldsymbol{\theta}\right) - \mathbf{x}\left(t\right)\right)$.

Also matrix $\mathbf{K}_c$ is a weight matrix: the higher the value of the stiffness associated to the i-th equation, the smaller the violation of the constraint $\gamma_i\left(\Delta\boldsymbol{\theta}\right) = x_i\left(t\right)$ that is allowed. In the limit case of $\mathbf{K}_i \to \infty$, the i-th driving constraint would not be violated.

This procedure enables the solution of the over-driven problem under investigation and allows the computation of vector $\boldsymbol{\theta}$ and its time derivatives $\dot{\boldsymbol{\theta}}$ and $\ddot{\boldsymbol{\theta}}$.

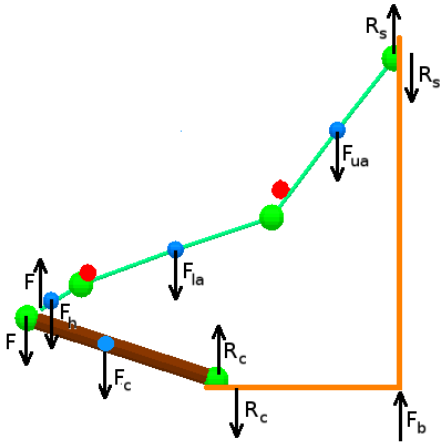

Figure 5: Sketch of the forces acting on the system.

3 POWER BALANCE APPROACH

An approach based on a power balance is proposed. The change in the total energy of an open system must be equal to the net power flow. When only mechanical energy is considered, under the assumption that thermodynamical changes can be neglected, the resulting equation can be used as the functional to be matched.

The power balance for the whole multibody system yields

$$\frac{\mathrm{d}E_k}{\mathrm{d}t} = \Pi_g + \Pi_b + \Pi_j, \tag{10}$$

where E_k is the kinetic energy, Π_g is the power of the gravitational forces, Π_b is the power needed to move the base and Π_j is the power associated to the deformable joints. This relationship is used to estimate Π_j and to indirectly identify the constitutive laws of the joints.

A multibody model of the problem allows to estimate the time derivative of the kinetic energy E_k from the measurements of the motion of the base, of the collective bar, and of the accelerations and angular velocities of the instrumented limbs by means of the MTx sensors,

$$\frac{\mathrm{d}E_k}{\mathrm{d}t} = \sum_{\text{body}} \left(\dot{\boldsymbol{\beta}} \cdot \dot{\mathbf{x}}_{\text{CM}} + \dot{\boldsymbol{\gamma}}_{\text{CM}} \cdot \boldsymbol{\omega} \right), \tag{11}$$

where the momentum $\boldsymbol{\beta}$, its time derivative $\dot{\boldsymbol{\beta}}$, the momenta moment $\boldsymbol{\gamma}_{\text{CM}}$ with respect to the center of mass, its time derivative $\dot{\boldsymbol{\gamma}}_{\text{CM}}$, the center of mass linear velocity $\dot{\mathbf{x}}_{\text{CM}}$ and the angular velocity $\boldsymbol{\omega}$ of the 4 rigid bodies of the arm model are standard outputs of the multibody code MBDyn.

The power of the gravitational forces is computed as:

$$\Pi_g(t) = \sum_{\text{body}} m\mathbf{g} \cdot \dot{\mathbf{x}}_{\text{CM}}, \tag{12}$$

where m is the mass of each body, estimated from the GEBOD database, and $\mathbf{g}$ is the gravity acceleration vector. The power contribution Π_b cannot be computed in a trivial way because the force needed to impose the base motion $\mathbf{f}_b$ is not known. However, from the sketch in Figure 5, the force $\mathbf{f}_b$ is

$$\mathbf{f}_b = \mathbf{r}_s + \mathbf{r}_c, \tag{13}$$

where $\mathbf{r}_s$ is the reaction force in the shoulder and $\mathbf{r}_c$ is the reaction in the collective hinge.

After defining $\mathbf{f}$ as the force exchanged between the collective bar and the hand, the reaction forces can be easily computed as

$$\mathbf{r}_s = -\mathbf{f} + \mathbf{f}_h + \mathbf{f}_l + \mathbf{f}_u, \tag{14}$$

where $\mathbf{f}_h$, $\mathbf{f}_l$ and $\mathbf{f}_u$ are the sum of the inertial and gravitational forces $\dot{\boldsymbol{\beta}}$ and $m\mathbf{g}$ respectively of the hand, lower arm and upper arm. Then

$$\mathbf{r}_c = \mathbf{f} + \mathbf{f}_c, \tag{15}$$

where $\mathbf{f}_c$ is the sum of inertial and gravitational force of the collective bar.

The power Π_b is then:

$$\begin{aligned} \Pi_b(t) &= \mathbf{f}_b \cdot \dot{\mathbf{x}}_b \\ &= (\mathbf{f}_h + \mathbf{f}_l + \mathbf{f}_u + \mathbf{f}_c) \cdot \dot{\mathbf{x}}_b \\ &= \sum_{body} \left(\dot{\boldsymbol{\beta}} + m\mathbf{g}\right) \cdot \dot{\mathbf{x}}_b, \end{aligned} \tag{16}$$

where $\dot{\mathbf{x}}_b$ is the velocity imposed to the base. Therefore the power Π_b does not depend on the unknown internal force $\mathbf{f}$ when the equilibrium of the whole system in the vertical direction is considered. Thus it can be computed by only knowing the inertial forces and the system movement.

Finally, the power associated to the deformable joints is:

$$\begin{aligned} \Pi_j(t) &= \frac{\mathrm{d}E_k}{\mathrm{d}t} - \Pi_g - \Pi_b \\ &= \sum_{\text{body}} \left(\left(\dot{\boldsymbol{\beta}} + m\mathbf{g}\right) \cdot (\dot{\mathbf{x}} - \dot{\mathbf{x}}_b) + \dot{\boldsymbol{\gamma}}_{\text{CM}} \cdot \boldsymbol{\omega} \right). \end{aligned} \tag{17}$$

From the expression of the power associated to the deformable joints, Π_j, as a function of the time t, the constitutive laws of the joints can be identified. First of a constitutive law structure must be assumed, namely

$$\mathbf{m}_a = \mathbf{f}\left(\boldsymbol{\theta}_a, \dot{\boldsymbol{\theta}}_a, \mathbf{p}\right), \tag{18}$$

where the joint moment $\mathbf{m}_a$ is function of the joint rotation $\boldsymbol{\theta}_a$, of the joint angular velocity $\dot{\boldsymbol{\theta}}_a$ and of some constitutive law parameters $\mathbf{p}$. The joint rotation $\boldsymbol{\theta}_a$ and rotation rate $\dot{\boldsymbol{\theta}}_a$ are standard outputs of the multibody simulation as well. The parameters $\mathbf{p}$ are obtained by minimizing the functional:

$$J = \frac{1}{2} \sum_k \left(\Pi_j(t_k) - \Pi_j^{\mathbf{p}}(t_k)\right)^2, \tag{19}$$

where $\Pi_j^{\mathbf{p}}$ is the expression of the power associated to the deformable joints as a function of the parameters $\mathbf{p}$:

$$\Pi_j^{\mathbf{p}}(t) = \sum_{\text{articulations}} \mathbf{m}_a\left(\boldsymbol{\theta}_a, \dot{\boldsymbol{\theta}}_a, \mathbf{p}\right) \cdot \dot{\boldsymbol{\theta}}_a. \tag{20}$$

For example, consider the identification of the parameters of a Linear Viscoelastic Isotropic (LVI) constitutive law for each joint. The assumed joint constitutive law is

$$\mathbf{m} = k\boldsymbol{\theta} + r\dot{\boldsymbol{\theta}}, \tag{21}$$

therefore 6 parameters need to be identified: the stiffness and damping coefficients of wrist, elbow and shoulder, respectively k_w, k_e, k_s, r_w, r_e e r_s.

The expression of the power $\Pi_j^{\mathrm{P}}(t)$ is

$$\Pi_j^{\mathrm{P}}(t) = \left[\begin{array}{cccccc} \theta_w \cdot \dot{\theta}_w & \theta_e \cdot \dot{\theta}_e & \theta_s \cdot \dot{\theta}_s & \dot{\theta}_w \cdot \dot{\theta}_w & \dot{\theta}_e \cdot \dot{\theta}_e & \dot{\theta}_s \cdot \dot{\theta}_s \end{array} \right] \left\{ \begin{array}{c} k_w \\ k_e \\ k_s \\ r_w \\ r_e \\ r_s \end{array} \right\}. \tag{22}$$

By evaluating the previous expression at each time step, one obtains the linear expression

$$\mathbf{\Pi}_j^{\mathrm{P}} = \mathbf{A}\mathbf{p}, \tag{23}$$

where the rows of matrix $\mathbf{A}$ are represented by the first multiplier at the right hand side of Eq. (22), evaluated at each time step. When this constitutive model is used, the minimization problem can be solved analytically as

$$\mathbf{p} = \left(\mathbf{A}^T\mathbf{A}\right)^{-1}\mathbf{A}^T\mathbf{\Pi}_j. \tag{24}$$

4 NUMERICAL RESULTS

4.1 Results without Measurement Noise

In order to test the identification procedure based on the power balance, a set of exact measures has been generated by a multibody simulation of the experiment, using arbitrary joint constitutive laws. This set of measures has been input into the identification procedure.

The procedure consists in performing a multibody dynamic analysis where:

- the collective rotation,
- the base motion,
- the motion of the two MTx sensors

are imposed. This allows to define the motion of the whole system in an appropriate manner. All the quantities needed to compute the power associated to the deformable joints are obtained as outputs from this analysis.

4.1.1 Linear Viscoelastic Isotropic Constitutive Law

The constitutive law for the 3 deformable joints is Linear Viscoelastic Isotropic (LVI):

$$\mathbf{m} = k\boldsymbol{\theta} + r\dot{\boldsymbol{\theta}}; \tag{25}$$

Table 4 shows the value of the 6 parameters that have been used during the simulation of the experiment. During the test simulation a movement of the base in the heave direction has been imposed, as in the real experiment. The input is a random signal filtered at 10 Hz. Figure 6 shows the input signal as a function of time. A smoothing transient has been added to improve the initial convergence of the multibody analysis. Figure 7 shows the frequency content of the input signal.

Table 4: LVI constitutive law parameters.

Joint	stiffness (k, Nm)	damping (r, Nms)
Wrist	99.1	0.991
Elbow	3.5	0.035
Shoulder	4.0	0.040

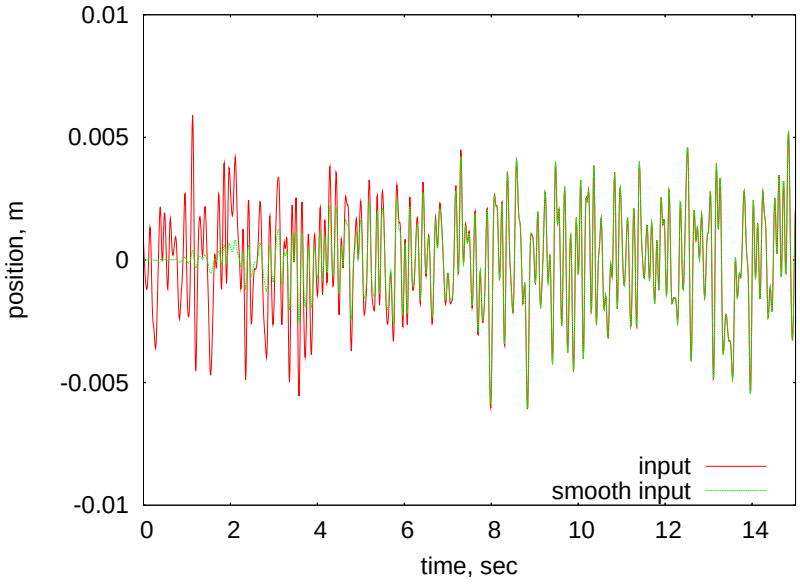

Figure 6: Seat vertical motion.

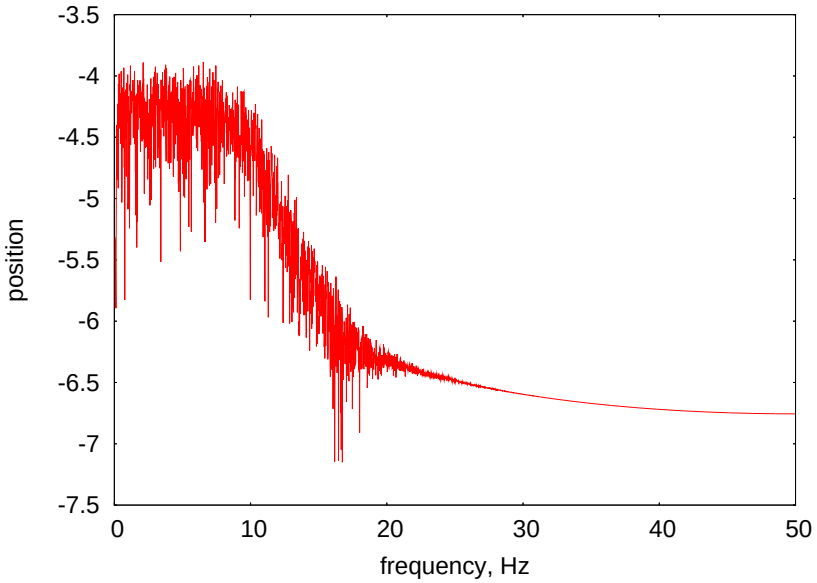

Figure 7: Seat vertical motion frequency content.

Table 5: Identified LVI constitutive law parameters (without gravity).

Joint		Imposed value	Identified value	Error, %
Wrist	stiffness, Nm	99.1	99.0806	-0.0196
	damping, Nms	0.991	0.9903	-0.0657
Elbow	stiffness, Nm	3.5	3.4994	-0.0178
	damping, Nms	0.035	0.035	0.0210
Shoulder	stiffness, Nm	4.0	4.0009	0.0220
	damping, Nms	0.04	0.0401	0.2343

Table 6: Identified LVI constitutive law parameters (with gravity).

Joint	Param.	Imp. val.	Id. val.	Err., %	Id. val.	Err., %
			CL1		CL2	
Wrist	k, Nm	99.1	90.2172	-8.9635	99.3978	0.3005
	r, Nms	0.991	0.8907	-10.1225	0.9905	-0.0519
	m_x, Nm	—	—	—	0.7201	—
	m_y, Nm	—	—	—	0.0491	—
Elbow	k, Nm	3.5	-5.1268	-246.48	3.4523	-1.3627
	r, Nms	0.035	0.0031	-91.0234	0.035	0.1213
	m_z, Nm	—	—	—	-0.0807	—
Shoulder	k, Nm	4.0	-1.225	-130.62	4.0146	0.3656
	r, Nms	0.04	0.4705	1076.3	0.0419	4.8496
	m_x, Nm	—	—	—	0.3126	—
	m_y	—	—	—	-5.3629	—
	m_z, Nm	—	—	—	-0.0045	—

Simulation without gravity. Table 5 shows the identification results when the experiment simulation is performed without gravity. Results are excellent and they show the correctness of the identification procedure based on the power balance.

Simulation with gravity. When gravity is added to the experiment simulation, the quality of the results degrades. Table 6 shows the results obtained using two constitutive laws for the identification:

identified value CL1: the identified constitutive law is linear viscoelastic isotropic:

$$\mathbf{m} = k\boldsymbol{\theta} + r\dot{\boldsymbol{\theta}}; \tag{26}$$

identified value CL2: the identified constitutive law is linear viscoelastic isotropic with a bias:

$$\mathbf{m} = \mathbf{m}_0 + k\boldsymbol{\theta} + r\dot{\boldsymbol{\theta}}; \tag{27}$$

The results of Table 6 show how the bias is required to obtain a good identification, otherwise the results are not physically meaningful because negative stiffness values appear. When gravity is considered, identification errors are larger but acceptable, provided bias is considered.

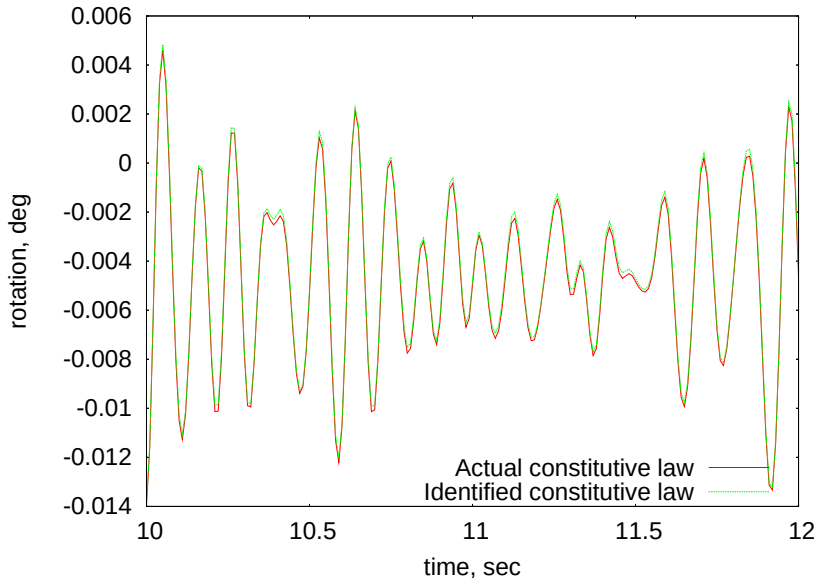

Figure 8: Comparison of the collective bar rotation obtained with the imposed and identified constitutive law parameters.

Table 7: Identified system poles (LVI constitutive law, with gravity).

Pole		Imposed value	Identified Value
Pole 1	frequency, Hz	3.71	3.78
	ξ, adim.	0.53	0.58
Pole 2	frequency, Hz	7.16	7.07
	ξ, adim.	0.34	0.34

Assessment of Results. In order to assess the quality of the results obtained with gravity, the experiment simulation has been repeated using the identified constitutive law. The resulting collective bar rotation has been compared to the rotation obtained with the initially imposed constitutive laws. Results are compared in Figure 8. The figure shows that the difference between the two signals is very small.

To further test the capabilities of the identified model to properly represent the relationship between the vertical motion of the pilot and the rotation of the collective bar, a fourth order state space model has been identified using a subspace method implemented in the System Identification Toolbox of Matlab [14].

The vertical motion of the pilot is the state space model input and the collective bar rotation is the output as obtained from the experiment simulation. A state space model is estimated from measurements obtained with the imposed and the identified constitutive law parameters. The poles of the two state-space models are compared in Table 7. The results show a good agreement both in terms of frequency and damping.

4.1.2 Linear Viscoelastic Orthotropic Constitutive Law

The identification procedure has also been tested with a more complex, Linear Viscoelastic Orthotropic (LVO) constitutive law:

Table 8: LVO constitutive law parameters.

Joint	direction	stiffness (k, Nm)	damping (r, Nms)
Wrist	x	100	3.00
	y	50	1.50
Elbow	z	3	0.06
Shoulder	x	15	0.15
	y	25	0.25
	z	35	0.35

Table 9: Identified LVO constitutive law parameters (without gravity).

Joint	Parameter	Imp. value	Id. value	Error, %
Wrist	k_x, Nm	100.0	99.29	-0.71
	k_y, Nm	50.0	51.88	3.76
	r_x, Nms	3.0	2.99	-0.31
	r_y, Nms	1.5	1.48	-1.36
Elbow	k_z, Nm	3.0	3.02	0.54
	r_z, Nms	0.06	0.0611	1.84
Shoulder	k_x, Nm	15.0	17.33	15.52
	k_y, Nm	25.0	67.62	170.48
	k_z, Nm	35.0	34.81	-0.53
	r_x, Nms	0.15	0.33	121.71
	r_y, Nms	0.25	0.50	101.23
	r_z, Nms	0.35	0.34	-1.71

- shoulder:

$$\left\{ \begin{array}{c} m_x \\ m_y \\ m_z \end{array} \right\} = \left\{ \begin{array}{c} m_{0x} \\ m_{0y} \\ m_{0z} \end{array} \right\} + \left[\begin{array}{ccc} k_x & 0 & 0 \\ 0 & k_y & 0 \\ 0 & 0 & k_z \end{array} \right] \left\{ \begin{array}{c} \theta_x \\ \theta_y \\ \theta_z \end{array} \right\} + \left[\begin{array}{ccc} r_x & 0 & 0 \\ 0 & r_y & 0 \\ 0 & 0 & r_z \end{array} \right] \left\{ \begin{array}{c} \dot{\theta}_x \\ \dot{\theta}_y \\ \dot{\theta}_z \end{array} \right\} \quad (28)$$

- elbow:

$$m_z = m_{0z} + k_z \theta_z + r_z \dot{\theta}_z; \quad (29)$$

- wrist:

$$\left\{ \begin{array}{c} m_x \\ m_y \end{array} \right\} = \left\{ \begin{array}{c} m_{0x} \\ m_{0y} \end{array} \right\} + \left[\begin{array}{cc} k_x & 0 \\ 0 & k_y \end{array} \right] \left\{ \begin{array}{c} \theta_x \\ \theta_y \end{array} \right\} + \left[\begin{array}{cc} r_x & 0 \\ 0 & r_y \end{array} \right] \left\{ \begin{array}{c} \dot{\theta}_x \\ \dot{\theta}_y \end{array} \right\}; \quad (30)$$

Table 8 shows the reference values of the parameters of the constitutive laws.

Simulation without gravity. Table 9 shows the identification results with measures obtained from a simulation where the constitutive laws are linear viscoelastic orthotropic, gravity is not present and excitation is only in the vertical direction.

The identified values of the parameters of the wrist and elbow constitutive laws show an error below 5%. The error is larger for the constitutive law of the shoulder, in particular for the

Table 10: Identified system poles (LVO constitutive law, without gravity, excitation only in the vertical direction).

Pole		Imposed value	Identified value
Pole 1	frequency, Hz	6.61	6.62
	ξ, adim.	0.33	0.34
Pole 2	frequency, Hz	11.62	11.59
	ξ, adim.	0.41	0.41

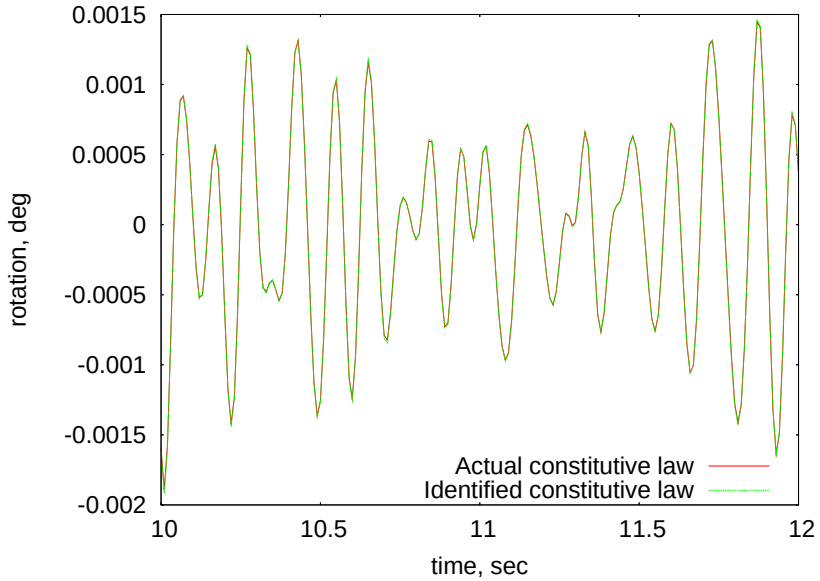

Figure 9: Comparison of the collective bar rotation obtained with the imposed and the identified constitutive laws.

parameters in the x and y directions. Despite the high identification error of some parameters, the model can adequately represent the relationship between the vertical motion of the pilot and the rotation of the collective bar. This is shown in Figure 9, where the collective bar rotation obtained with the imposed and the identified constitutive laws parameters are compared (they can be hardly distinguished), and in Table 10, where the poles of the state space model identified from the two responses are compared.

The poorly identified parameters appear to have a negligible impact on the relationship between the vertical motion and the collective bar rotation. The quality of the identification improves when the system is simultaneously excited in all the directions during the simulation of the experiment. The identified parameters in this latter case are shown in Table 11.

Simulation with gravity. When gravity is considered, the quality of the identified values of the constitutive laws parameters is very similar to that obtained without gravity, as shown in Table 12. When all directions are simultaneous excited, the quality of the results improves. In any case, the parameters that are poorly identified do not significantly affect the response, as shown in Table 13.

4.2 Measurement Noise

In real experiments measures are always affected by measurement noise. Noisy measures may not be consistent from the point of view of kinematics. Problems related to this inconsis-

Table 11: Identified LVO constitutive law parameters (without gravity, excitation in all directions).

Joint	Parameter	Imp. value	Id. value	Error, %
Wrist	k_x, Nm	100.0	100.16	0.16
	k_y, Nm	50.0	50.03	0.06
	r_x, Nms	3.0	3.00	-0.058
	r_y, Nms	1.5	1.49	-0.76
Elbow	k_z, Nm	3.0	3.01	0.17
	r_z, Nms	0.06	0.0604	0.63
Shoulder	k_x, Nm	15.0	16.51	10.04
	k_y, Nm	25.0	19.70	-21.20
	k_z, Nm	35.0	34.92	-0.23
	r_x, Nms	0.15	0.27	80.14
	r_y, Nms	0.25	0.07	-70.81
	r_z, Nms	0.35	0.345	-1.32

Table 12: Identified LVO constitutive law parameters (with gravity).

Joint	Par.	Imp. val.	Id. val.	Err., %	Id. val.	Err., %
			Z exc.		XYZ exc.	
Wrist	k_x, Nm	100.0	97.82	-2.18	100.19	0.19
	k_y, Nm	50.0	62.10	24.19	48.95	-2.10
	r_x, Nms	3.0	2.99	-0.28	2.99	-0.35
	r_y, Nms	1.5	1.46	-2.63	1.50	0.19
	m_{0x}, Nm	—	-0.39	—	0.34	—
	m_{0y}, Nm	—	0.13	—	0.074	—
Elbow	k_z, Nm	3.0	2.85	-5.05	2.93	-2.19
	r_z, Nms	0.06	0.0614	2.31	0.0608	1.26
	m_{0z}, Nm	—	-0.19	—	-0.12	—
Shoulder	k_x, Nm	15.0	-14.38	-195.88	25.75	71.69
	k_y, Nm	25.0	110.95	343.81	24.49	-2.02
	k_z, Nm	35.0	36.03	2.93	34.53	-1.35
	r_x, Nms	0.15	0.56	270.36	0.14	-8.60
	r_y, Nms	0.25	0.54	114.68	0.66	166.09
	r_z, Nms	0.35	0.34	-4.12	0.35	-0.0044
	m_{0x}, Nm	—	0.91	—	0.50	—
	m_{0y}, Nm	—	2.90	—	-2.52	—
	m_{0z}, Nm	—	-0.29	—	-0.10	—

Table 13: Identified system poles (LVO constitutive law, with gravity).

Pole		Imp. value	Id. val.-Z exc.	Id. val.-XYZ exc.
Pole 1	frequency, Hz	6.15	6.39	6.34
	ξ, adim.	0.35	0.34	0.35
Pole 2	frequency, Hz	11.89	11.74	11.77
	ξ, adim.	0.39	0.44	0.44

tency arise when a redundant set of measures is used to impose the motion of the whole system. This occurs when the position and the rotation of the 2 MTx sensors placed on the arm and on the forearm are simultaneously imposed.

In this case the inconsistent set of measures can be preprocessed by a kineto-static multibody simulation to obtain a consistent set, as described in the next section.

4.3 Kinematic Compatibility by Inverse Kinematics

The inverse kinematics simulation, explained from a theoretical point of view in subsection 2.4.1, is performed to transform an inconsistent set of measures into a consistent one. After preprocessing, the consistent set of measures is input into the identification procedure described in Section 3.

The inverse kinematics analysis consists in a static simulation where the measured signals are not directly imposed to the collective bar and to the two MTx sensors, but rather to additional nodes, connected to the related bodies by elastic elements. The motion of the whole system is tuned by modifying the stiffness of these elastic connection elements.

The outputs of this simulation are the placement of the hand holding the collective bar and the arm and forearm motion in the points where the sensors are placed. The measures obtained from this procedure intrinsically comply with the kinematic constraints.

4.4 Results with Noisy Measures

Two signals are added to the arm and forearm position and orientation measurements:

- a random bias;
- a low-pass filtered random signal.

In order to test the inverse kinematics effectiveness the constitutive laws are identified in two different ways:

ID using the noisy measures as input for the identification procedure;

ID+KIN preprocessing the noisy measures with the inverse kinematics simulation and using these preprocessed measures as input for the identification procedure.

Identification is performed in presence of gravity, with excitation only in the heave direction and using linear viscoelastic constitutive laws. The parameters of the constitutive laws are again those summarized in Table 4.

Figure 10 compares the exact and the noisy measures. Even if the noise level is low, the identification error is greater than the error obtained with the exact measures.

Preprocessing the measures for kinematic compliance reduces the identification error, as shown in Table 14. The poles of the system identified from the vertical pilot motion and the collective bar rotation, shown in Table 15, are significantly incorrect, especially the low frequency one, unless preprocessing is used.

Using an higher noise level the identification quality worsens. Table 16 shows the results for the noise level shown in Figure 12. In this case the results obtained without preprocessing the measures are definitely unsatisfactory, as shown also in Table 17. The results for the identification without the inverse kinematics preprocessing are not even computed because the multibody simulation with the identified constitutive laws parameters does not converge.

Further increment of the noise level leads to the impossibility to obtain significant results, not even after preprocessing the signals by means of inverse kinematics analysis.

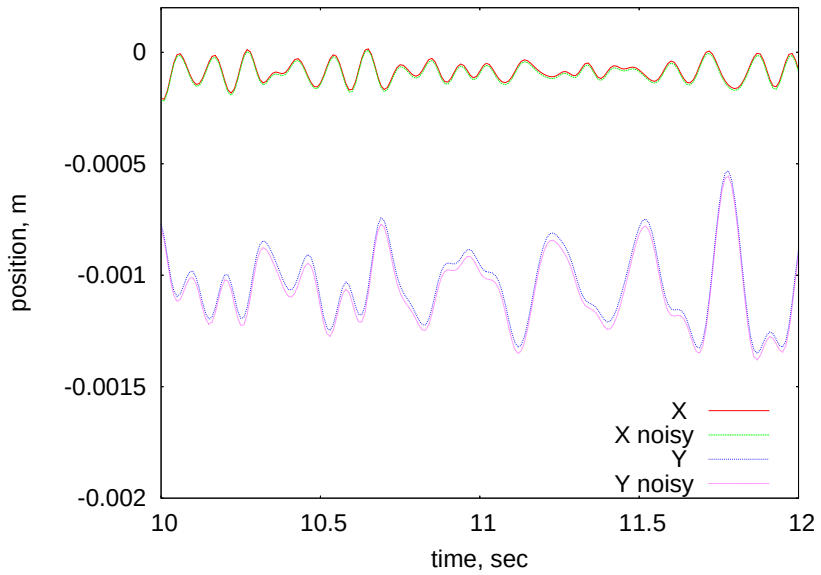

Figure 10: Comparison of the exact and noisy position measurements in the X and Y direction (low noise level).

Table 14: Identified constitutive law parameters with a low noise level.

Joint	Param.	Imp. val.	Id. val. ID	Err., % ID	Id. val. ID+KIN	Err., % ID+KIN
Wrist	k, Nm	99.1	96.29	-2.8	97.42	-1.69
	r, Nms	0.991	1.0225	3.18	0.9882	-0.29
	m_{0x}, Nm	—	-2.35	—	-1.6185	—
	m_{0y}, Nm	—	-0.9115	—	-0.2038	—
Elbow	k, Nm	3.5	2.796	-20.11	3.2593	-6.88
	r, Nms	0.035	0.033	-5.82	0.0343	-1.90
	m_{0z}, Nm	—	-0.1669	—	-0.2711	—
Shoulder	k, Nm	4.0	3.1999	-20.00	4.5192	12.98
	r, Nms	0.04	0.039	-2.42	0.0426	6.45
	m_{0x}, Nm	—	-2.9975	—	0.2392	—
	m_{0y}, Nm	—	12.4088	—	11.1424	—
	m_{0z}, Nm	—	0.2267	—	-0.3353	—

Table 15: Identified system poles (low noise level).

Pole		Imp. value	Id. value, ID	Id. value, ID+KIN
Pole 1	frequency, Hz	3.30	3.76	3.39
	ξ, adim.	0.41	0.85	0.35
Pole 2	frequency, Hz	7.38	6.13	7.04
	ξ, adim.	0.33	0.33	0.39

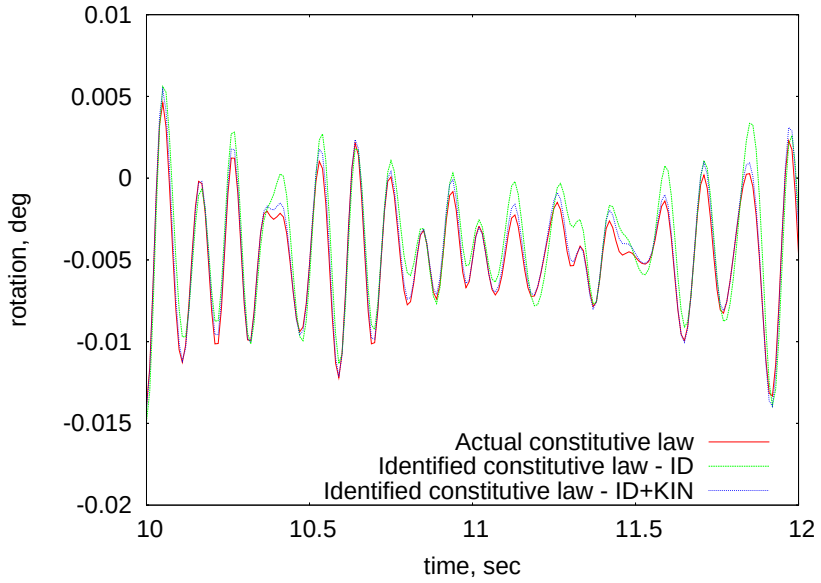

Figure 11: Comparison of the collective bar rotation obtained with the imposed and the identified constitutive laws.

Table 16: Identified constitutive law parameters with a high level of noise.

Joint	Param.	Imp. val.	Id. val. ID	Err., % ID	Id. val. ID+KIN	Err., % ID+KIN
Wrist	k, Nm	99.1	54.68	-44.82	91.51	-7.66
	r, Nms	0.991	0.7713	-22.17	0.9849	-0.61
	m_{0x}, Nm	—	-6.978	—	-3.3998	—
	m_{0y}, Nm	—	-2.1393	—	0.4342	—
Elbow	k, Nm	0.5683	2.796	-83.76	3.1311	-10.54
	r, Nms	0.0466	0.033	33.16	0.0296	-15.43
	m_{0z}, Nm	—	-0.4075	—	-0.4679	—
Shoulder	k, Nm	4.0	-2.4531	-161.33	3.6490	-8.78
	r, Nms	0.04	-0.0119	-129.78	0.0182	-54.59
	m_{0x}, Nm	—	-14.0243	—	0.9587	—
	m_{0y}, Nm	—	49.7886	—	24.9748	—
	m_{0z}, Nm	—	1.4438	—	-0.7704	—

Table 17: Identified system poles (high noise level).

Pole		Imposed value	Id. value, ID	Id. value, ID+KIN
Pole 1	frequency, Hz	3.30	—	3.40
	ξ, adim.	0.41	—	0.29
Pole 2	frequency, Hz	7.38	—	6.77
	ξ, adim.	0.33	—	0.31

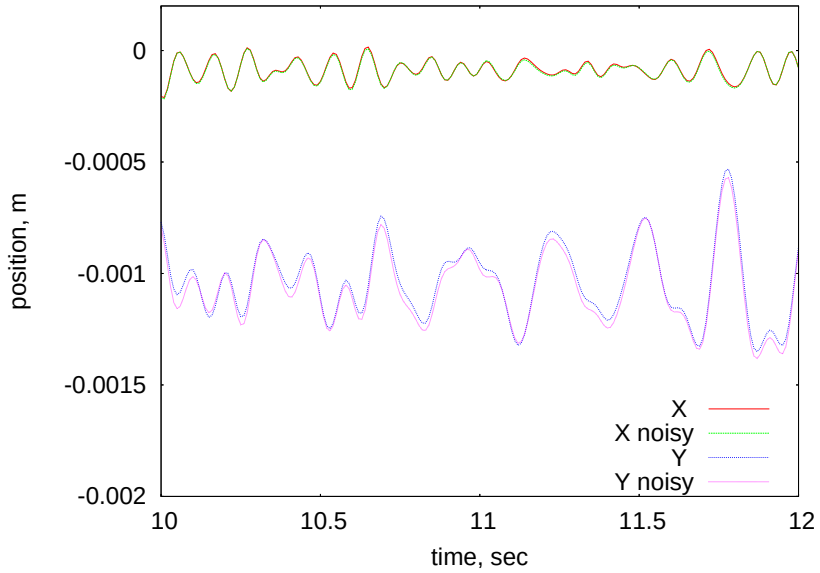

Figure 12: Comparison of the exact and noisy position measurements in the X and Y directions (high noise level).

5 Conclusions

The proposed identification technique gives good results in absence of measurement noise. This illustrates the correctness of the underlying idea. Unfortunately this technique is not robust enough with respect to the measurement noise and it tolerates only low levels of noise.

Because of the limited robustness the proposed technique was unable to identify reasonable constitutive parameters from experimental measurements using relatively simple constitutive models. It is worth stressing that in the real case there may be multiple sources of model uncertainty that are not present in the simulated environment, like:

- the arm anthropomorphic characteristics are estimated from the GEBOD database, so they might not correspond exactly to the characteristics of the subjects of the experimental tests;
- the initial position of the MTx sensors is not perfectly known;
- the MTx position measure is obtain by means of a double integration of the measured acceleration;
- the structure of the actual constitutive laws is not known, so it needs to be chosen a priori.

Further investigation and model refinement is required to be able to fit the experimental data with an acceptable agreement.

REFERENCES

[1] D. T. McRuer. *Aviation Safety and Pilot Control: Understanding and Preventing Unfavourable Pilot-Vehicle Interactions*. Washington DC: National Research Coucil, National Academy Press, 1997.

[2] R. Barry Walden. A retrospective survey of pilot-structural coupling instabilities in naval rotorcraft. In *63rd Annual Forum of the American Helicopter Society*, Virginia Beach, VA, May 1–3 2007.

[3] Henry R. Jex and Raymond E. Magdaleno. Biomechanical models for vibration feedthrough to hands and head for a semisupine pilot. *Aviation, Space and Environmental Medicine*, January 1978.

[4] Gordon Hoehne. A biomechanical pilot model for prediction of roll ratcheting. In *AIAA Atmospheric Flight Mechanics Conference and Exhibit*, Portland, OR, August 9–11 1999. AIAA–1999–4092.

[5] John R. Mayo. The involuntary participation of a human pilot in a helicopter collective control loop. In *15th European Rotorcraft Forum*, pages 81.1–12, Amsterdam, The Netherlands, 12–15 September 1989.

[6] Tom Parham Jr. and David Popelka. V–22 pilot-in-the-loop aeroelastic stability analysis. In *47th Annual Forum of the American Helicopter Society*, Phoenix, Arizona (USA), May 6–8 1991.

[7] Pierangelo Masarati, Giuseppe Quaranta, Walter Basso, Riccardo Bianco-Mengotti, and Claudio Monteggia. Biodynamic tests for pilots' characterization on the BA–609 fly-by-wire tiltrotor. In *XX AIDAA Congress*, Milano, Italy, June 29-July 3 2009.

[8] O. Dieterich, J. Götz, B. DangVu, H. Haverdings, P. Masarati, M. Pavel, M. Jump, and M. Gennaretti. Adverse rotorcraft-pilot coupling: Recent research activities in europe. In *34th European Rotorcraft Forum*, Liverpool, UK, September 16–19 2008.

[9] M. Gennaretti, J. Serafini, P. Masarati, G. Quaranta, and O. Dieterich. Aeroelastic and biodynamic modeling for stability analysis of rotorcraft-pilot coupling phenomena. In *34th European Rotorcraft Forum*, Liverpool, UK, September 16–19 2008.

[10] M. Mattaboni, A. Fumagalli, M. Jump, P. Masarati, and G. Quaranta. Biomechanical pilot properties identification by inverse kinematics/inverse dynamics multibody analysis. In *ICAS-International Council for the Aeronautical Sciences*, Anchorage, Alaska, USA, September 14–19 2008.

[11] M. Jump, S. Hodge, B. DangVu, P. Masarati, G. Quaranta, M. Mattaboni, M. Pavel, and O. Dieterich. Adverse rotorcraft-pilot coupling: The construction of the test campaigns at the university of liverpool. In *34th European Rotorcraft Forum*, Liverpool (UK), September 16–19 2008.

[12] Huaining Cheng, Louise Obergefell, and Annette Rizer. Generator of body (GEBOD) manual. Technical Report AL/CF-TR-1994-0051, Air Force Materiel Command, Wright-Patterson Air Force Base, Ohio, 1994.

[13] A. Fumagalli, G. Gaias, and P. Masarati. A simple approach to kinematic inversion of redundant mechanisms. In *IDETC/CIE 2007 ASME 2007 International Design Engineering Technical Conferences & Computers and Information in Engineering Conference*, Las Vegas, Nevada, USA, September 4–7 2007.

[14] Matlab System Identification Toolbox. Technical report, The Mathworks. http://www.mathworks.com/.